




Cite this: *Chem. Sci.*, 2023, 14, 5125

All publication charges for this article have been paid for by the Royal Society of Chemistry

# Molecular engineering of locked alkyl aryl carbonyl-based thermally activated delayed fluorescence emitters via a cascade C–H activation process†

Yunxi Zhang, Zhengmei Huang, Yudong Yang,  Jiahui Liu, Yang Tian, Zhengyang Bin \* and Jingsong You \*

While diaryl ketones have drawn tremendous attention for the assembly of carbonyl-based thermally activated delayed fluorescence (TADF) emitters, alkyl aryl ketones are almost ignored. In this work, an efficient rhodium-catalyzed cascade C–H activation process of alkyl aryl ketones with phenylboronic acids has been developed for the concise construction of the  $\alpha,\alpha$ -dialkyl/aryl phenanthrene skeleton, which unlocks an opportunity to rapidly assemble a library of structurally nontraditional locked alkyl aryl carbonyl-based TADF emitters. Molecular engineering indicates that the introduction of a donor on the A ring enables the emitters to exhibit better TADF properties than those with a donor on the B ring. 2,6-Bis(9,9-dimethylacridin-10(9H)-yl)-10,10-diphenylphenanthren-9(10H)-one (2,6-DMAC-DPPO) with two donors on the A and B rings gives rise to superior organic light-emitting diode (OLED) performance with maximum external quantum efficiency and power efficiency as high as 32.6% and 123.5 lm W<sup>-1</sup>, respectively.

Received 10th March 2023

Accepted 18th April 2023

DOI: 10.1039/d3sc01298k

rsc.li/chemical-science

## Introduction

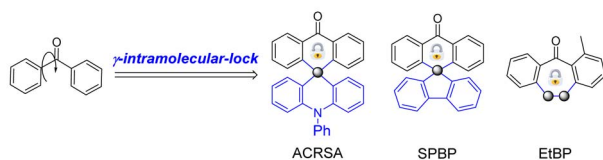
Thermally activated delayed fluorescence (TADF) has emerged as one of the most promising exciton-harvest mechanisms to achieve 100% theoretical exciton utilization efficiency in organic light-emitting diodes (OLEDs), and thus is the current hotspot in both scientific community and OLED industry.<sup>1</sup> The benzophenone (BP) unit is a highly electron-deficient diaryl carbonyl framework, in which the n-orbital of the carbonyl group enables enhancement of the spin–orbital coupling and thus efficiently promotes the up-conversion process.<sup>2</sup> The BP unit has widely been used as the acceptor to construct efficient TADF molecules since Adachi and co-workers firstly reported an efficient BP acceptor-based TADF emitter.<sup>3</sup> The acyclic conformation of the BP acceptor has good rotatability, which renders the corresponding TADF molecules with an aggregation-induced emission (AIE) effect to reduce exciton quenching in the aggregated state,<sup>4</sup> but the acyclic configuration inevitably causes molecular friction by excessive structural relaxation, which leads to nonradiative decay. Thus, further development

of the molecular design concept for improving the device performance of carbonyl-based TADF emitters is highly desired yet remains a challenging issue. Recently, the  $\gamma$ -intramolecular-lock strategy of diaryl carbonyl acceptors has been considered as an effective method to construct high-performance carbonyl-based TADF materials (Scheme 1a), which not only enables the suppression of intermolecular Dexter energy transfer to reduce exciton quenching, but also restricts excessive rotation to inhibit structural relaxation.<sup>5</sup> For example, Adachi and co-workers developed a spiro-anthracenone-based TADF sensitizer (ACRSA) to assemble high-performance fluorescence OLEDs.<sup>6</sup> Recently, Zhang and co-workers reported a  $\gamma$ -C(sp<sup>3</sup>) locked SPBP acceptor and further constructed efficient TADF emitters for non-doped OLEDs.<sup>7</sup> You and co-workers designed a heptagonal BP skeleton (EtBP) with a flexible  $\gamma$ -ethylidene lock that was applied as an efficient bipolar host for phosphorescent OLEDs.<sup>8</sup>

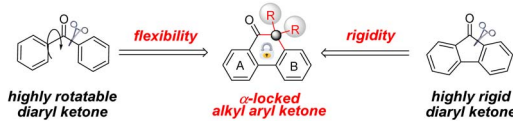
While diaryl ketones have drawn tremendous attention, alkyl aryl ketones are almost ignored for use in the construction of carbonyl-based TADF emitters. Inspired by our “medium-ring acceptor” strategy,<sup>8,9</sup> we propose a brand-new type of locked alkyl aryl carbonyl acceptor for developing structurally nontraditional carbonyl-based TADF emitters (Scheme 1b). This strategy cuts off a carbonyl–aryl bond and introduces a C(sp<sup>3</sup>) center to form the  $\alpha,\alpha$ -dialkyl/aryl phenanthrene fragment. The locked geometry endows the acceptor with a delicate balance between flexibility and rigidity, which enables restraint of the excessive intramolecular rotation, and meanwhile enables

Key Laboratory of Green Chemistry and Technology of Ministry of Education, College of Chemistry, Sichuan University, 29 Wangjiang Road, Chengdu 610064, People's Republic of China. E-mail: binzhengyang@scu.edu.cn; yjsou@scu.edu.cn

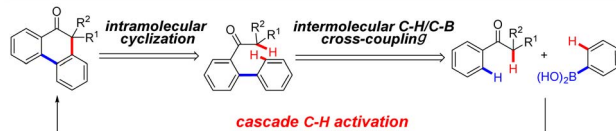
† Electronic supplementary information (ESI) available: Experimental details, crystallographic data, theoretical calculation, photophysical performances, thermal and electrochemical properties of the compounds. CCDC 2241220 (2-DMAC-DPPO) and 2241219 (2,6-DMAC-DMPO). For ESI and crystallographic data in CIF or other electronic format see DOI: <https://doi.org/10.1039/d3sc01298k>

a) Previous work of  $\gamma$ -intramolecular-lock strategy for diaryl carbonyl acceptor

## b) Molecular design concept for locked alkyl aryl carbonyl acceptor



- More efficient to protect the carbonyl from the intermolecular interactions
- Induced intramolecular hydrogen-bonding interaction to restrict structural relaxation
- Delicate balance between flexibility and rigidity

c) Synthetic strategy for  $\alpha,\alpha$ -dialkyl/aryl phenanthrone

Scheme 1 Molecular design of locked alkyl aryl ketone acceptors for the construction of efficient TADF emitters.

suppression of the close intermolecular  $\pi$ - $\pi$  stacking. Compared with the  $\gamma$ -locked diaryl carbonyl acceptor, the  $\alpha$ -locked alkyl aryl carbonyl acceptor with alkyl- or aryl groups adjacent to the carbonyl center possesses a similar energy level alignment (Fig. S1†), but is proposed to be more effective to protect the carbonyl group from the close intermolecular interactions, so as to reduce exciton quenching. In addition, the introduction of rotatable methyl- or phenyl-protection groups adjacent to the carbonyl center would also potentially induce intramolecular hydrogen-bonding interactions (Fig. S1†), so as to restrict structural relaxation and thus enhance radiative decay. With the concept in mind, we herein wish to present the

systematic molecular engineering, including the molecular design, the concise synthesis of emitters and the screening of high-performance OLEDs.

## Results and discussion

### Reaction development

To test our proposal, it is undoubtedly required to develop a general and streamlined synthetic strategy to rapidly access the locked alkyl aryl carbonyl acceptors and assemble a rich library of TADF molecules.

From the retrosynthesis analysis, the cascade C-H activation processes involving the intermolecular Ar-H/Ar-B cross-coupling and the sequential intramolecular Ar-H/C(sp<sup>3</sup>)-H cyclization would provide a straightforward route to forge the locked  $\alpha,\alpha$ -dialkyl/aryl phenanthrone skeleton (Scheme 1c).<sup>10</sup> In the synthetic strategy, the carbonyl unit is not only used as a directing group, but also directly constitutes the acceptor fragment. The prerequisite to achieve this cascade process is that the optimized reaction condition should be simultaneously compatible with the two different types of coupling reactions. In addition, these two types of oxidative C-H activation reactions are needed to tolerate reactive halogen groups on both substrates, which is beneficial for the further construction of TADF molecules. We initiated our investigation by using 2-methyl-1-phenylpropan-1-one (**1a**) and phenylboronic acid (**2a**) as the model substrates (Table 1). In a [Cp\*RhCl<sub>2</sub>]<sub>2</sub>/AgSbF<sub>6</sub> catalyst system, the  $\alpha,\alpha$ -dimethyl phenanthrone product **3a** was obtained in 66% yield by using Cu(OAc)<sub>2</sub> as the oxidant, 1,2-dichloroethane (DCE) as the solvent and pivalic acid (PivOH)/sodium trifluoromethane-sulfonate (NaOTf) as the additive (Table 1, entry 1). Further screening of catalysts, oxidants and solvents reveals that the replacement of [Cp\*RhCl<sub>2</sub>]<sub>2</sub>/AgSbF<sub>6</sub>, Cu(OAc)<sub>2</sub> and DCE did not give rise to a higher yield (Table 1, entries 2–6). The mixed PivOH/NaOTf as the additive was superior to PivOH, NaOTf or sodium acetate (NaOAc) (Table 1,

Table 1 Optimization of the reaction conditions<sup>a</sup>

Entry	Variation from the standard conditions	Yield <sup>b</sup> [%]
1	None	66
2	Without [Cp*RhCl <sub>2</sub> ] <sub>2</sub> /AgSbF <sub>6</sub>	N.R.
3	Without Cu(OAc) <sub>2</sub>	N.R.
4	[RhCp*(MeCN) <sub>3</sub> (SbF <sub>6</sub> ) <sub>2</sub> ] instead of [Cp*RhCl <sub>2</sub> ] <sub>2</sub> /AgSbF <sub>6</sub>	31
5	Dioxane, THF, DCM instead of DCE	8, 5, 45
6	AgNO <sub>3</sub> , Cu(NO <sub>3</sub> ) <sub>2</sub> , Cu(acac) <sub>2</sub> instead of Cu(OAc) <sub>2</sub>	8, N.R., 16
7	Without PivOH/NaOAc	<5
8	PivOH, NaOTf, NaOAc instead of PivOH/NaOTf	44, 60, 33
9	PivOH/NaOAc, PivOH/NaOAc instead of PivOH/NaOTf/NaOTf	72 <sup>c</sup> , 84 <sup>d</sup>

<sup>a</sup> Reaction conditions: **1a** (0.2 mmol), **2a** (0.6 mmol), [Cp\*RhCl<sub>2</sub>]<sub>2</sub> (5.0 mol%), AgSbF<sub>6</sub> (20 mol%), Cu(OAc)<sub>2</sub> (2.0 equiv.), PivOH (0.5 equiv.), NaOTf (0.5 equiv.) and DCE (1.0 mL) at 150 °C for 24 h under N<sub>2</sub>. <sup>b</sup> The yield was determined by <sup>1</sup>H NMR analysis of the crude product using CH<sub>2</sub>Br<sub>2</sub> as an internal standard. <sup>c</sup> PivOH (1.0 equiv.) and NaOAc (0.2 equiv.). <sup>d</sup> PivOH (1.2 equiv.) and NaOAc (0.2 equiv.). DCM = dichloromethane.



entries 7 and 8). To our delight, the product **3a** was afforded in a higher yield of 72% with PivOH/NaOAc as the additive, and when using 1.2 equiv. PivOH and 0.2 equiv. NaOAc, the yield was elevated to 84% (Table 1, entry 9). It is worthy of note that only trace amounts of the intermediate **3a'** were monitored under the optimized reaction conditions, revealing a high efficiency of the subsequent intramolecular Ar–H/C(sp<sup>3</sup>)–H cyclization.

### Reaction scope

With the optimized reaction conditions in hand, we next examined the generality of substrate. As summarized in Scheme 2, a variety of alkyl aryl ketones (**1**) and arylboronic acids (**2**) smoothly participated in this cascade process to deliver a variety of  $\alpha,\alpha$ -dialkyl/aryl phenanthrones (**3**) in moderate to excellent yields. To our delight, this reaction was tolerant of halogens (e.g., fluoro, chloro and bromo) at different sites and was successfully extended to  $\alpha,\alpha$ -diphenyl,  $\alpha$ -methyl- $\alpha$ -phenyl and  $\alpha$ -cyclopentyl substrates, which exhibits the potential for the rapid construction of structurally diverse TADF molecules. Moreover, to investigate the synthetic applicability of this reaction, a 1.0 mmol scale reaction was conducted to afford dihalogenated product **3j** in 67% yield.

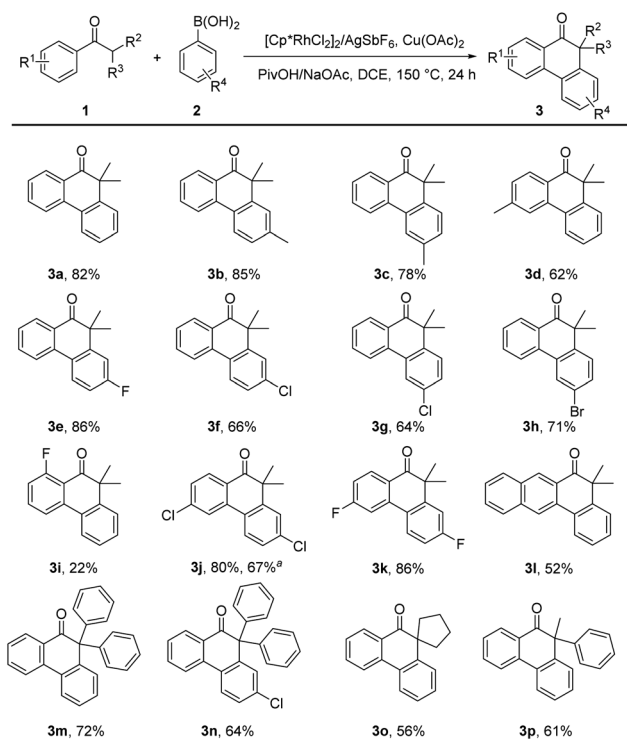
### Assembly of TADF emitters

With a library of 10,10-dimethylphenanthren-9(10*H*)-one-methane (DMPO) and 10,10-diphenylphenanthren-9(10*H*)-one-

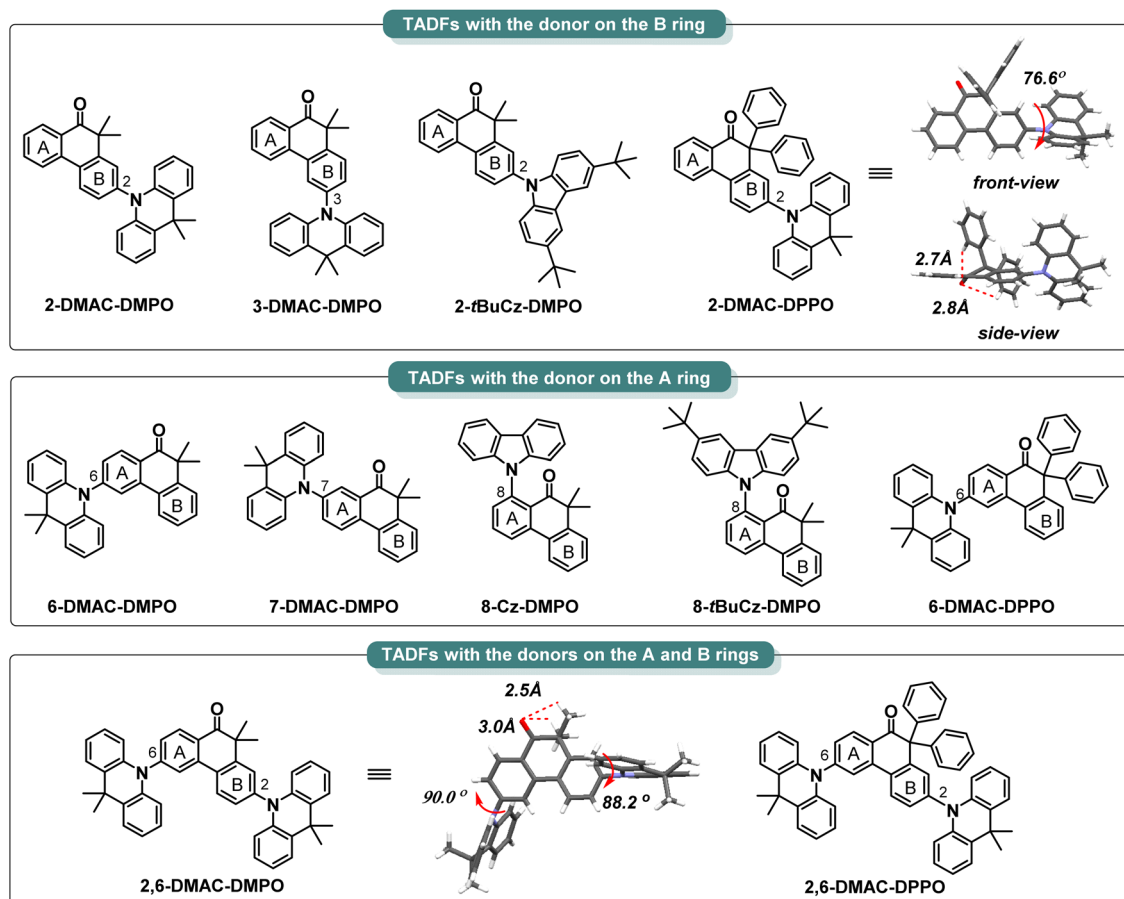
methane (DPPO) skeletons in hand, we tried to assemble structurally diverse TADF molecules by utilizing 9,9-dimethyl-9,10-dihydroacridine (DMAC), carbazole (Cz) and 3,6-di-*tert*-butyl-carbazole (*t*BuCz) as the donors (Scheme 3). The halogen-substituted DMPO and DPPO skeletons underwent the Buchwald–Hartwig amination or the nucleophilic substitution with the DMAC, Cz or *t*BuCz donor to rapidly access a spectrum of designed compounds (for synthetic details, see Part VII†). The crystals of **2,6-DMAC-DMPO** and **2-DMAC-DPPO** were obtained during the temperature gradient vacuum sublimation process, and the corresponding crystal structures are shown in Scheme 3.† **2,6-DMAC-DMPO** and **2-DMAC-DPPO** both display highly twisted molecular structures with large dihedral angles of 88.2° and 90.0° between the DMAC donor and the DMPO acceptor in **2,6-DMAC-DMPO** and of 76.6° between the DMAC donor and the DPPO acceptor in **2-DMAC-DPPO**. Moreover, obvious intramolecular C–H⋯O hydrogen-bonding interactions exist between the  $\alpha$ -methyl groups and the carbonyl group with the distances of 2.5 Å and 3.0 Å in **2,6-DMAC-DMPO** and between the  $\alpha$ -phenyl groups and the carbonyl group with the distances of 2.7 Å and 2.8 Å in **2-DMAC-DPPO**, which are beneficial to restrict structural relaxation and thus enhance radiative decay.

### Thermal, electrochemical and photophysical performances

The photophysical performances of the designed compounds were investigated systematically and are summarized in Fig. 1 and Table 2. All compounds display obvious shoulder absorption peaks at 350–450 nm, and the optical energy band gap ( $E_g$ ) calculated from the longest absorption wavelengths ranges from 2.74 eV to 3.04 eV (Fig. 1a and Table 2). In the fluorescence spectra measured in toluene solution, these compounds exhibit broad and featureless charge-transfer emissions (<sup>1</sup>CT). Compared with **8-Cz-DMPO** and **8-*t*BuCz-DMPO** that possess the donors *ortho* to the carbonyl group, the other TADF molecules exhibit more significantly red-shifted emissions with the increased polarity of the solvents, indicative of the stronger CT characters (Fig. S2†). Moreover, we also observed that the emitters with the donor on the A ring (e.g., **6-DMAC-DMPO**, **7-DMAC-DMPO**, **8-Cz-DMPO**, **8-*t*BuCz-DMPO** and **6-DMAC-DPPO**) display significantly red-shifted emissions compared to those with the donor on the B ring (e.g., **2-DMAC-DMPO**, **3-DMAC-DMPO**, **2-*t*BuCz-DMPO** and **2-DMAC-DPPO**) (Fig. 1b and Table 2), which is probably due to the lower unoccupied molecular orbital (LUMO) distributions on the A ring compared to those on the B ring (Fig. S3†) that facilitate the CT emissions. However, the phosphorescence spectra of these compounds are well-resolved and show vibrational structures, and the emissions are almost identical (Fig. 1c), revealing that their triplet states belonging to localized excited states (<sup>3</sup>LE) mainly reside on the DMPO or DPPO acceptors according to the theoretical calculations (Fig. S3†). Thus, these compounds possess similar triplet energy levels ( $E_{T1}$ , Table 2). In contrast, due to the stronger CT characters and thus more significantly red-shifted emissions, the emitters with the donor on the A ring possess considerably lower singlet energy levels ( $E_{S1}$ , Table 2) than the emitters with the donor on the B ring. As a result, the emitters



**Scheme 2** Scope of substrates. Reaction conditions: **1** (0.2 mmol), **2** (0.6 mmol), [Cp\*RhCl<sub>2</sub>]<sub>2</sub> (5.0 mol%), AgSbF<sub>6</sub> (20 mol%), Cu(OAc)<sub>2</sub> (2.0 equiv.), PivOH (1.2 equiv.), NaOAc (0.2 equiv.) and DCE (1.0 mL) at 150 °C for 24 h under N<sub>2</sub>. Isolated yields. <sup>a</sup> 1.0 mmol scale.



Scheme 3 Molecular structures of designed TADF molecules by utilizing DMPO or DPPO as the acceptor.

with the donor on the A ring possess a significantly smaller  $\Delta E_{ST}$  value ranging from 0.01 eV to 0.04 eV than those with the donor on the B ring (0.16 eV to 0.52 eV), indicative of the better TADF properties. In addition, the transient photoluminescence spectra measured for the widely used bis[2-(diphenylphosphino)phenyl]ether oxide (DPEPO) host-based films also reveal that the emitters with the donor on the A ring display better TADF properties with significantly shorter delayed lifetimes ranging from 1.3  $\mu$ s to 8.4  $\mu$ s than those with the donor on the B ring (132.1  $\mu$ s to 160.6  $\mu$ s; Fig. 1d and Table 2).

In dilute tetrahydrofuran (THF) solutions, most of the compounds display relatively weak photoluminescence with low PLQY, and the photoluminescence intensities are greatly enhanced upon the addition of a poor solvent (water) into the THF solution, revealing the aggregation-induced emission (AIE) properties that are beneficial to the high PLQY in the aggregated states (Fig. 1e, f and S4<sup>†</sup>). For example, the PLQY values of **6-DMAC-DMPO** and **6-DMAC-DPPO** in the DPEPO host-blended films (75.3% and 74.6%, respectively) are significantly higher than those in the dilute toluene solutions (5.3% and 7.5%, respectively) (Table 2). Intriguingly, the introduction of an auxiliary donor on the 2-position of **6-DMAC-DMPO** and **6-DMAC-DPPO** enables further increase of the PLQY values of the doped films (94.3% for **2,6-DMAC-DMPO** and 90.1% for **2,6-DMAC-DPPO**), while maintaining small  $\Delta E_{ST}$  values (0.04 eV for

**2,6-DMAC-DMPO** and 0.01 eV for **2,6-DMAC-DPPO**). The higher PLQY values of **2,6-DMAC-DMPO** and **2,6-DMAC-DPPO** than those of **6-DMAC-DMPO** and **6-DMAC-DPPO** are possibly attributed to the increased HOMO delocalization by multiple donor as well as the more twisted donor-acceptor-donor molecular geometry to suppress the ACQ effect in the film (Fig. S3<sup>†</sup>).<sup>12</sup>

Among the TADF molecules, **6-DMAC-DMPO**, **2,6-DMAC-DMPO**, **6-DMAC-DPPO** and **2,6-DMAC-DPPO** with a DMAC donor on the A ring simultaneously possess small  $\Delta E_{ST}$  values and high PLQY values. Therefore, they are further used as the emitters to assemble OLEDs, and their electroluminescence performances were investigated. **2-DMAC-DPPO** is chosen for comparison. Prior to the device fabrication, the thermal and electronic properties of these compounds were measured. The smooth thermogravimetric analysis (TGA) curves indicate that these compounds possess good thermal stability with high decomposition temperature at 5% weight loss ( $T_d$ ) ranging from 333 °C to 409 °C, which is beneficial for the vacuum-deposited OLED fabrication process (Fig. S5<sup>†</sup> and Table 2). The highest occupied molecular orbital (HOMO) energies of these compounds were measured by cyclic voltammetry (CV, Fig. S6<sup>†</sup>), which range from −5.34 eV to −5.03 eV, and the LUMO energies were calculated from the HOMO energies and the  $E_g$  values, which range from −2.43 eV to −2.16 eV (Table 2).





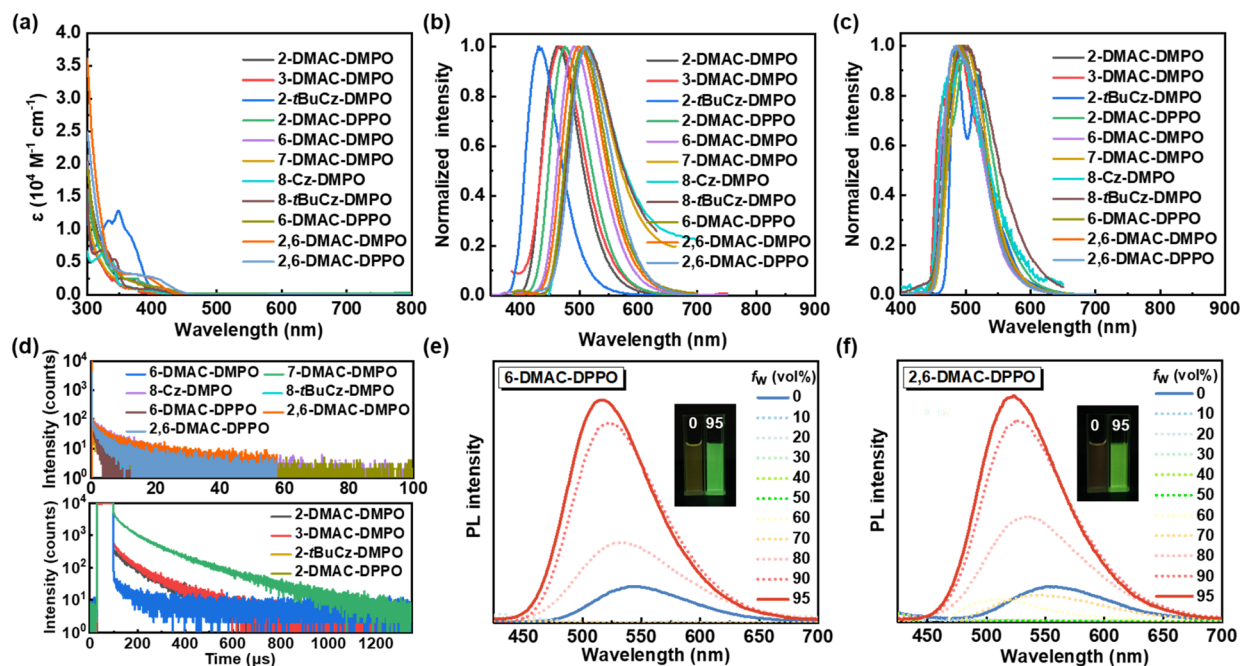


Fig. 1 (a) Absorption (at room temperature), (b) fluorescence (at room temperature) and (c) phosphorescence (at 77 K) spectra of the designed compounds in toluene solution ( $1.0 \times 10^{-5}$  M). (d) Transient photoluminescence spectra of the designed compounds in DPEPO host-blended film (40 wt%) at room temperature. Fluorescence spectra of (e) 6-DMAC-DPPO and (f) 2,6-DMAC-DPPO in THF/water mixtures with different water fractions ( $f_w$ ). Insets in (e) and (f): photographs of 6-DMAC-DPPO (e) and 2,6-DMAC-DPPO (f) in THF/water mixtures ( $f_w = 0$  and 95%) under 365 nm excitation.

## OLED performance

OLEDs were assembled using 6-DMAC-DMPO, 2,6-DMAC-DMPO, 6-DMAC-DPPO, 2,6-DMAC-DPPO and 2-DMAC-DPPO as the emitters and DPEPO as the host. The optimized device structure is ITO/1,1-bis[(di-4-tolylamino)phenyl]cyclohexane (TAPC, 10 or 25 or 35 nm)/tris(4-carbazolyl-9-ylphenyl)amine (TCTA, 5 nm)/emitter: host (40%, 35 nm)/4,7-diphenyl-1,10-phenanthroline (BPhen, 55 nm)/LiF (0.8 nm)/Al (100 nm)

(Fig. S7†). The device performances are summarized in Fig. 2 and Table 3. All the devices display low turn-on voltages ranging from 2.5 V to 2.9 V (Fig. 2d) and green emissions with emission peaks ( $EL_{peak}$ ) ranging from 508 nm to 545 nm (Fig. 2c), indicating the sufficient energy transfer from the DPEPO host to the emitters. Compared with 6-DMAC-DMPO and 6-DMAC-DPPO, 2,6-DMAC-DMPO and 2,6-DMAC-DPPO with two donors exhibit superior electroluminescence performances with high

Table 2 Summary of thermal, electrochemical and photophysical performance

Donor	Emitter	$T_d$ [°C]	HOMO <sup>a</sup> [eV]	LUMO <sup>b</sup> [eV]	$E_g^c$ [nm]	$\lambda_{em,sol}^d$ [nm]	$\lambda_{em,film}^e$ [nm]	$E_{S1}^f$ [eV]	$E_{T1}^g$ [eV]	$\Delta E_{ST}^h$ [eV]	$\Phi_{PL,sol}^i$ [%]	$\Phi_{PL,film}^e$ [%]	$\tau_d^e$ [μs]
On the B ring	2-DMAC-DMPO	—	−5.06	−2.04	3.02	463	470	3.00	2.76	0.24	5.7	17.7	145.0
	3-DMAC-DMPO	—	−5.03	−2.00	3.03	466	470	3.01	2.79	0.22	3.3	5.7	143.4
	2- <i>t</i> BuCz-DMPO	—	−5.33	−2.29	3.04	431	450	3.17	2.65	0.52	5.5	18.0	132.1
	2-DMAC-DPPO	370	−5.34	−2.43	2.91	475	500	2.89	2.73	0.16	9.6	42.6	160.6
On the A ring	6-DMAC-DMPO	333	−5.08	−2.27	2.81	490	510	2.80	2.76	0.04	5.3	75.3	7.8
	7-DMAC-DMPO	—	−5.32	−2.47	2.85	511	510	2.74	2.72	0.02	8.4	27.0	8.4
	8-Cz-DMPO	—	−5.36	−2.48	2.88	512	496	2.77	2.74	0.03	1.9	1.5	1.7
	8- <i>t</i> BuCz-DMPO	—	−5.48	−2.67	2.81	515	496	2.75	2.73	0.02	7.2	5.2	1.3
On the A and B rings	6-DMAC-DPPO	381	−5.07	−2.33	2.74	506	522	2.79	2.78	0.01	7.5	74.6	4.5
	2,6-DMAC-DMPO	404	−5.03	−2.16	2.87	498	516	2.78	2.74	0.04	7.0	94.3	10.5
	2,6-DMAC-DPPO	409	−5.08	−2.32	2.76	511	522	2.74	2.73	0.01	13.0	90.1	4.2

<sup>a</sup> Measured in dry DCM at  $1.0 \times 10^{-3}$  M containing 0.1 M of tetrabutylammonium hexafluorophosphate. <sup>b</sup>  $E_{LUMO} = E_{HOMO} + E_g$ . <sup>c</sup> Energy gap calculated from the longest wavelength in the absorption spectrum. <sup>d</sup> Measured in toluene solution ( $1.0 \times 10^{-5}$  M) at room temperature. <sup>e</sup> Measured in DPEPO host-blended film (40 wt%) at room temperature. <sup>f</sup> Calculated from the onset wavelength of the fluorescence spectrum at room temperature. <sup>g</sup> Calculated from the onset wavelength of the phosphorescence spectrum at 77 K. <sup>h</sup> Calculated from  $E_{S1}$  and  $E_{T1}$ . <sup>i</sup> Measured in toluene solution ( $1.0 \times 10^{-5}$  M) in a  $N_2$  atmosphere at room temperature.

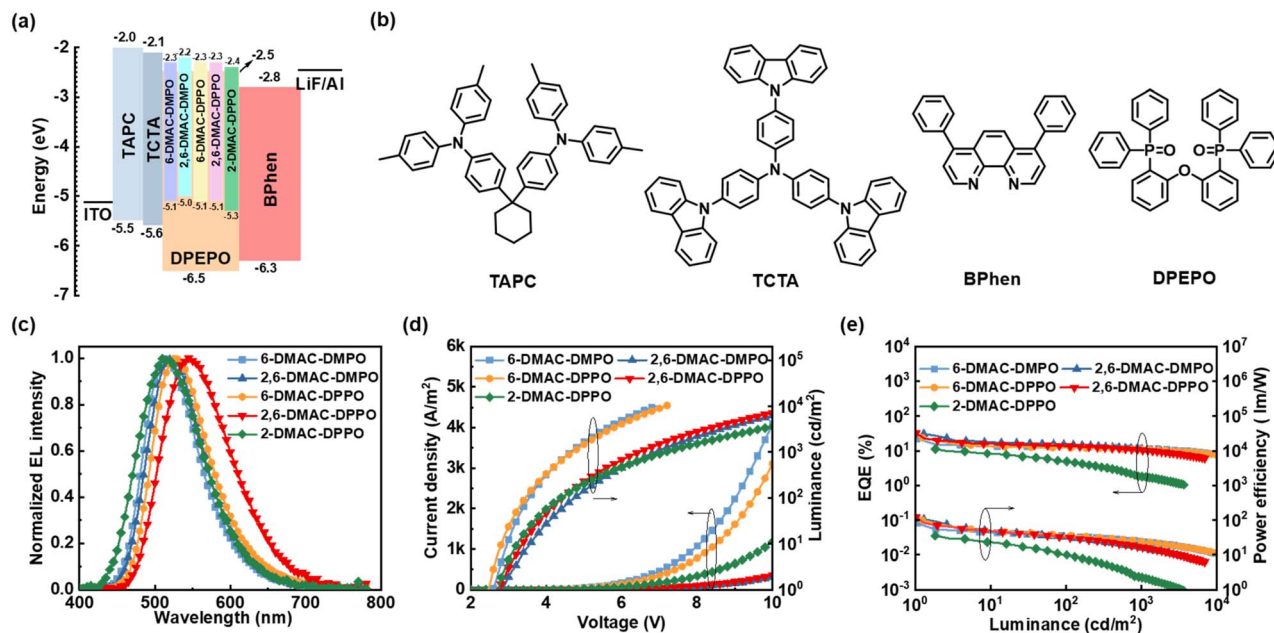


Fig. 2 (a) Energy level diagrams and (b) molecular structures of the materials used in OLEDs. (c) Electroluminescence spectra at 1000  $\text{cd m}^{-2}$ . (d) Current density–voltage–luminance curves and (e) EQE–luminance–power efficiency curves of OLEDs.

Table 3 Summary of OLED performances

Emitter	EL <sub>peak</sub> <sup>a</sup> [nm]	CIE <sup>b</sup> [x, y]	V <sub>on</sub> [V]	CE <sub>max</sub> [ $\text{cd A}^{-1}$ ]	EQE <sub>max</sub> [%]	PE <sub>max</sub> [ $\text{lm W}^{-1}$ ]
6-DMAC-DMPO	508	[0.27, 0.55]	2.6	67.9	22.4	82.1
2,6-DMAC-DMPO	521	[0.29, 0.56]	2.9	99.2	31.0	107.4
6-DMAC-DPPO	526	[0.32, 0.58]	2.5	79.1	24.0	99.5
2,6-DMAC-DPPO	545	[0.39, 0.55]	2.7	106.2	32.6	123.5
2-DMAC-DPPO	515	[0.27, 0.49]	2.8	31.9	11.2	35.8

<sup>a</sup> EL<sub>peak</sub> measured at 1000  $\text{cd m}^{-2}$ . <sup>b</sup> Commission Internationale de l'Eclairage (CIE) 1931 coordinates measured at 1000  $\text{cd m}^{-2}$ .

maximum current efficiencies ( $\text{CE}_{\text{max}}$ ) of 99.2  $\text{cd A}^{-1}$  and 106.2  $\text{cd A}^{-1}$ , maximum external quantum efficiencies ( $\text{EQE}_{\text{max}}$ ) of 31.0% and 32.6% and maximum power efficiencies ( $\text{PE}_{\text{max}}$ ) of 107.4  $\text{lm W}^{-1}$  and 123.5  $\text{lm W}^{-1}$  (Fig. 2e). These results represent one of the state-of-the-art performances for the reported carbonyl-based TADF molecules (Table S5†). In contrast, relatively low efficiencies were measured for the 2-DMAC-DPPO-based device ( $\text{CE}_{\text{max}}$  of 31.9  $\text{cd A}^{-1}$ ,  $\text{EQE}_{\text{max}}$  of 11.2% and  $\text{PE}_{\text{max}}$  of 35.8  $\text{lm W}^{-1}$ ).

## Conclusions

In summary, we have developed an efficient rhodium-catalyzed cascade C–H activation process of alkyl aryl ketones with phenylboronic acids for the construction of the  $\alpha,\alpha$ -dialkyl/aryl phenanthrone skeleton. This concise synthetic strategy provides an opportunity to rapidly access structurally nontraditional locked alkyl aryl carbonyl-based TADF emitters. With small  $\Delta E_{\text{ST}}$  values of 0.04 eV and 0.01 eV as well as high PLQY values of 94.3% and 90.1%, 2,6-DMAC-DMPO and 2,6-DMAC-

DPPO are successfully utilized as the emitters to assemble high-performance OLEDs. This work not only demonstrates the potential of  $\alpha$ -locked alkyl aryl carbonyl acceptors for the construction of efficient TADF molecules and further assembly of high-performance OLEDs, but also showcases the superiority of the C–H activation method as an easy toolbox for the development of a library of OLED materials.

## Author contributions

Y. Zhang carried out most parts of the experiments. Z. Huang performed theoretical calculations. J. Liu and Y. Tian measured the electrochemical properties. Y. Zhang, Y. Yang, Z. Bin and J. You wrote the manuscript. Z. Bin and J. You supervised the research. All authors contributed to the discussion of the results.

## Conflicts of interest

There are no conflicts to declare.



## Acknowledgements

We acknowledge financial support from the National Natural Science Foundation of China (No. 22031007, 22005204, 22275127 and 22171188) and the Natural Science Foundation of Sichuan Province (No. 2022NSFSC0295). We thank Dr Shaolan Wang (Analytical & Testing Center, Sichuan University) for assistance with thermogravimetric measurements.

## Notes and references

- (a) H. Uoyama, K. Goushi, K. Shizu, H. Nomura and C. Adachi, *Nature*, 2012, **492**, 234–240; (b) Y. Tao, K. Yuan, T. Chen, P. Xu, H. Li, R. Chen, C. Zheng, L. Zhang and W. Huang, *Adv. Mater.*, 2014, **26**, 7931–7958; (c) M. Y. Wong and E. Zysman-Colman, *Adv. Mater.*, 2017, **29**, 1605444; (d) G. Hong, X. Gan, C. Leonhardt, Z. Zhang, J. Seibert, J. M. Busch and S. Bräse, *Adv. Mater.*, 2021, **33**, 2005630.
- (a) S. Aloïse, C. Ruckebusch, L. Blanchet, J. Réhault, G. Buntinx and J.-P. Huvenne, *J. Phys. Chem. A*, 2008, **112**, 224–231; (b) W. Zhao, Z. He, J. W. Y. Lam, Q. Peng, H. Ma, Z. Shuai, G. Bai, J. Hao and B. Z. Tang, *Chem*, 2016, **1**, 592–602.
- (a) Q. Zhang, D. Tsang, H. Kuwabara, Y. Hatae, B. Li, T. Takahashi, S. Y. Lee, T. Yasuda and C. Adachi, *Adv. Mater.*, 2015, **27**, 2096–2100; (b) J. Huang, H. Nie, J. Zeng, Z. Zhuang, S. Gan, Y. Cai, J. Guo, S.-J. Su, Z. Zhao and B. Z. Tang, *Angew. Chem., Int. Ed.*, 2017, **56**, 12971–12976; (c) J. Guo, X.-L. Li, H. Nie, W. Luo, S. Gan, S. Hu, R. Hu, A. Qin, Z. Zhao, S.-J. Su and B. Z. Tang, *Adv. Funct. Mater.*, 2017, **27**, 1606458; (d) H. Liu, J. Zeng, J. Guo, H. Nie, Z. Zhao and B. Z. Tang, *Angew. Chem., Int. Ed.*, 2018, **57**, 9290–9294; (e) P. Sharif, E. Alemdar, S. Ozturk, O. Caylan, T. Hacıfendioglu, G. Buke, M. Aydemir, A. Danos, A. P. Monkman, E. Yildirim, G. Gunbas, A. Cirpan and A. Oral, *Adv. Funct. Mater.*, 2022, **32**, 2207324; (f) M. R. Nagar, K. Kumar, D. Blazelevicius, R. Beresneviciute, G. Krucaite, D. Tavgeniene, C. T. Hao, S. Banik, J.-H. Jou and S. Grigalevicius, *J. Mater. Chem. C*, 2023, **11**, 1579–1592.
- J. Mei, N. L. C. Leung, R. T. K. Kwok, J. W. Y. Lam and B. Z. Tang, *Chem. Rev.*, 2015, **115**, 11718–11940.
- B. Li, M. Liu, L. Sang, Z. Li, X. Wan and Y. Zhang, *Adv. Opt. Mater.*, 2023, 2202610.
- H. Nakanotani, T. Higuchi, T. Furukawa, K. Masui, K. Morimoto, M. Numata, H. Tanaka, Y. Sagara, T. Yasuda and C. Adachi, *Nat. Commun.*, 2014, **5**, 4016.
- L. Wu, K. Wang, C. Wang, X.-C. Fan, Y.-Z. Shi, X. Zhang, S.-L. Zhang, J. Ye, C.-J. Zheng, Y.-Q. Li, J. Yu, X.-M. Oua and X.-H. Zhang, *Chem. Sci.*, 2021, **12**, 1495–1502.
- W. Ma, Z. Bin, G. Yang, J. Liu and J. You, *Angew. Chem., Int. Ed.*, 2022, **61**, e202116681.
- (a) Z. Huang, Z. Bin, R. Su, F. Yang, J. Lan and J. You, *Angew. Chem., Int. Ed.*, 2020, **59**, 9992–9996; (b) Z. Huang, B. Lei, D. Yang, D. Ma, Z. Bin and J. You, *Angew. Chem., Int. Ed.*, 2022, **61**, e202213157; (c) B. Lei, Z. Huang, S. Li, J. Liu, Z. Bin and J. You, *Angew. Chem., Int. Ed.*, 2023, e202218405.
- (a) X. Qin, X. Li, Q. Huang, H. Liu, D. Wu, Q. Guo, J. Lan, R. Wang and J. You, *Angew. Chem., Int. Ed.*, 2015, **54**, 7167–7170; (b) Y. Yang, J. Lan and J. You, *Chem. Rev.*, 2017, **117**, 8787–8863; (c) B. Li, A. I. M. Ali and H. Ge, *Chem*, 2020, **6**, 2591–2657; (d) K. Wang, J. Zhang, R. Hu, C. Liu, T. A. Bartholome, H. Ge and B. Li, *ACS Catal.*, 2022, **12**, 2796–2820.
- CCDC 2241220 (2-DMAC-DPPO) and CCDC 2241219 (2,6-DMAC-DMPO) contain the supplementary crystallographic data for this paper.†
- (a) C. Duan, J. Li, C. Han, D. Ding, H. Yang, Y. Wei and H. Xu, *Chem. Mater.*, 2016, **28**, 5667–5679; (b) Y. Im, M. Kim, Y. J. Cho, J.-A. Seo, K. S. Yook and J. Y. Lee, *Chem. Mater.*, 2017, **29**, 1946–1963; (c) T.-L. Wu, M.-J. Huang, C.-C. Lin, P.-Y. Huang, T.-Y. Chou, R.-W. Chen-Cheng, H.-W. Lin, R.-S. Liu and C.-H. Cheng, *Nat. Photonics*, 2018, **12**, 235–240.

